Carbon Trends 13 (2023) 100296

Contents lists available at ScienceDirect

Carbon Trends

journal homepage: www.elsevier.com/locate/cartre

Dual emitting carbon nanoparticles for tunable white light emission

Ann Mary K A [a,1,*], Tessy Paul [a,1], Anupama Kuttappan [a], Jibin P O [a], Anoop K K [b]

[a] Department of Physics, St. Thomas College (Autonomous), Thrissur 680 001, India
[b] Department of Physics, Cochin University of Science & Technology, Cochin, Kerala 680 022, India

ARTICLE INFO

Keywords:
White light emitting devices (WLEDS)
Carbon nanoparticles
Dual emission
Tunable CCT values

ABSTRACT

Eco-friendly, biomass derived single component luminescent materials with dual emission bands hold immense potential in white light emitting devices (WLED). Compared to WLED fabricated from different color emitting carbon nanoparticles, self-reabsorption and degradation will be negligible in single system white light emitting materials which guarantees stability in long run. Herein, we report a facile, inexpensive and sustainable direct thermal decomposition method to synthesize carbon nanoparticles with dual emission bands. Addition of PVP could efficiently enhance the red emission band of carbon nanoparticles. The excitation dependent broad blue-green emission and excitation independent narrow red emission helps to obtain white light emitting carbon nanoparticles. Upon change in excitation wavelength from 410 nm to 370 nm, white light emissions are obtained with tunable CCT value from 2648 K to 8980 K respectively. By virtue of this tunable warm to cool white light emission, single system WLED can be designed suitable for both indoor and outdoor applications.

1. Introduction

Over the last few decades a sudden upsurge in the research of white light emitting materials occurred owing to their application in solid state lighting [1,2] displays [3] and fluorescent sensors [4]. Conventional white illumination systems use careful controlling of red-green-blue (RGB) color profiles of individual light emitting phosphor devices [5]. An alternate way for efficient white light perception is to coat suitable rare-earth phosphor materials on a single chip [6]. However, design, complexity, low reproducibility rate for color tuning, low color rendering index (CRI) and relatively higher color correlated temperatures (CCT) hamper with their routine applications [5,7]. Deepening concerns regarding the depleting sources of rare earth materials, their cost effectiveness and compatibility with the environment has also triggered minds to search for suitable alternatives [8]. Currently, great deal of efforts is put into white light emitting devices (WLEDs) exploiting various photophysical properties of semiconductor quantum dots [9, 10], nanomaterials [11–13], polymers [14], metal-organic frameworks (MOFs) [15,16], lanthanide doped systems [17] and organic-inorganic hybrids [18,19].

Carbon based nanomaterials are often exploited for their hassle free and facile synthesis, low cost, biocompatibility, excellent photoluminescence (PL) properties and high stability in various devices [20–22]. Extensive studies are done on these materials to understand the mechanism of photoluminescence, their correlation to the structure and synergistic contribution of various optical active centres [23,24]. Their sp^2 hybridised graphitic core with varying surface appendages has always been rigorously studied for application in catalysis [25], sensors [26,27], imaging [28] and other optoelectronic devices. Mn doped carbon dots with strong pH responsive blue, green and orange fluorescence were utilized for white light emission (WLE) in a recent work [29]. Nitrogen and phosphorous doped carbon quantum dots synthesized by a one pot microwave route were reported to have a strong single WLE in solution as well as polymer frame [30]. Chen et al. recently reported a double band carbon nanostructures formed from the hydrothermal synthesis of 1,3-dihydroxynaphthalene and hydrochloric acid [31]. The single white light converter obtained was fabricated into a solid state WLED exhibiting a cold light source with CIE values (0.3122, 0.3429). However, adjustable white light emission parameters and CCT values with different excitation wavelengths from a single component material is still a matter to explore.

Nevertheless, most of these reports use complex and skill demanding synthesis procedures and even costly carbon and amine precursors [24, 32]. Natural sources being cheap, environment friendly with hassle free extraction procedures and strong fluorescence could pose as an alternative to such lab-grown inorganic luminogens [33,34]. An aqueous dye

* Corresponding author.
E-mail address: annmaryka@stthomas.ac.in (A.M. K A).
[1] Contributed equally.

https://doi.org/10.1016/j.cartre.2023.100296
Received 7 July 2023; Received in revised form 8 September 2023; Accepted 13 September 2023
Available online 15 September 2023

cocktail with pomegranate and curcumin extract in ethanol was recently used for WLE [35]. Though there are a few prior works in natural dye and dye derived quantum dots for WLE, these mostly use mixed emitter tuning [36,37]. Stable and highly photoluminescent carbon nanoparticles synthesized by a one pot thermal degradation with panchromatic emission remains conceptual and enigmatic to date.

Herein, we report dual emitting carbon nanoparticles produced from the leaves of *Hemigraphis colorata* for White Light Emission (WLE). Commonly known as the red flame ivy, these exotic perennial herbs belonging to the Acanthaceae family are often exploited for their anti-inflammatory, antibacterial and wound healing potencies [38,39]. Its dye extract was reportedly used as a photosensitizer in combination with mesoporus TiO_2 for photovoltaic application [40]. A one step, facile low temperature thermal decomposition route is adopted which can ensure easy, large scale, inexpensive and sustainable synthesis. The optical properties, Commission Internationale d'Eclairage (CIE) coordinates and CCT values of the fluorescent nanoparticles are calculated. Encapsulation of the nanoparticles in a matrix like silica xerogel could inhibit undesirable aggregation induced quenching (AIQ) in the nanomaterials, prevent degradation and facilitate easy device fabrication.

2. Experimental section

2.1. Materials

Fresh *Hemigraphis colorata* leaves were picked from the home garden. The leaves were washed thoroughly with water and air-dried prior to use. Polyvinyl pyrrolidone (PVP, MW=40,000) was bought from standard sources and used without any further purification. Distilled water was used throughout the experiment.

2.2. Characterization

The X-Ray Diffraction (XRD) analysis was done on Aeris Research XRD Diffractometer, (PANalytical, The Netherlands) with a scanning range of $2\theta = 10-90^{\circ}$ with Cu Kα radiation ($\lambda = 1.540598$ Å). The surface functional groups were identified from Fourier-transform infrared (FT-IR) spectra recorded in transmission mode on a FTIR spectrometer (Thermo Nicolet, USA) at room temperature in the range 4000–400 cm^{-1}. A high-resolution transmission electron microscopy (HRTEM) data using a TALOS F200S G2 transmission electron microscope (200 kV, FEG, CMOS Camera 4 K × 4 K) was used to identify the morphology of the sample. Ultraviolet/Visible (UV/Vis) absorption spectra in the range 200–700 nm were obtained from the Shimadzu UV 1800 spectrophotometer. All photoluminescence measurements were made on a Fluorolog NIR spectrofluorometer (Horiba Jobin Yvon, USA). WLED properties like color rendering index (CRI), color coordinate (CIE), and correlated color temperature (CCT) were evaluated from *Color Calculator* software.

2.3. Synthesis of carbon nanoparticles (CNP)

The carbon nanoparticles were synthesized through direct thermal decomposition of the precursor. The leaves of *Hemigraphis colorata* were washed, air-dried at room temperature and crushed using a mortar and pestle to obtain fine powder. 1 g of PVP was dissolved in 200 mL distilled water. 10 g of leaf powder was added to the above solution and agitated homogeneously. The mixture was kept in the oven at 95 °C for 24 h and then allowed to cool naturally to room temperature. The solution was filtered using a Whatman filter paper and dark brown supernatant solution obtained (CNP) was used for further experiments. The carbon nanoparticles made in a similar manner without adding PVP was named CN.

3. Results and discussion

The XRD pattern (Fig. 1a) of CNP shows a wide peak centered at 2*theta* value of 23°. This suggests the graphitic structure of the nanoparticles corresponding to (002) plane [41]. FTIR spectrum (Fig. 1b) helps to identify the surface functional groups and moieties attached to the graphitic core. The broad band from 3050 to 3550 cm^{-1} can be attributed to the stretching vibrations of hydrophilic groups –OH and –NH. These surface groups are responsible for water dispersibility of the synthesized nanoparticles. The bands peaked at 580, 1636, 2080 cm^{-1} correspond to –OH bending vibration, stretching vibration of –C=O, -C-N, respectively [42]. This confirms that the structural skeleton of CNP contains electron donating groups and porphyrin groups attached to the surface or core.

The morphology of the sample was studied by Transmission Electron Microscopy (TEM). Fig. 2a shows monodispersed quasi spherical carbon nanoparticles in PVP polymer. The statistical particle size histogram (Fig. 2b) evaluated from the TEM image shows a distribution in the range of 28–42 nm.

EDX spectrum (Fig. 3) reveals that CNP contains C, N, O, Mg, Cl, Ca. Presence of magnesium indicates the existence of chlorophyll within the dual emissive CNPs. Also, peaks corresponding to Cl and Ca are observed due to trace amount of elements present in leaf.

The optical properties of CNP were studied from UV-visible and fluorescence spectra as shown in Fig. 4a. The absorption spectrum of CNP has characteristic bands corresponding to the electronic transition in carbon centres and surface states. The strong band centered at 336 nm can be attributed to n→π* edge transition of the aromatic sp^2 -C=O bond in nanocarbon [43]. It is primarily responsible for surface trapping of excited energy and the blue emission mostly observed in carbon cores. To gain better insights into the role of PVP on the optical properties of synthesized nanoparticles, carbon nanoparticles were prepared without using PVP (CN). Similar to UV-visible spectrum of CNP, band peaked at 333 nm can be attributed to n→π* transitions of the aromatic sp^2 carbon system [43]. In CNP, the absorption bands in the visible region (400–700 nm) are mainly due to the transitions of surface groups [44]. The absorption bands at 405 and 655 nm can be ascribed to the π →π* and n→π* electron transition (Soret band and Q-band) of the -C=O and -C=N bonds in the chlorophyll-derived porphyrin [45,46]. For CN, weak absorption band in the visible region suggests that lack of PVP results in less surface passivation with nitrogen-containing molecules. The fluorescence spectra of CN and CNP exhibit dual and distinct emission bands at ~480 and 665 nm upon UV excitations (Fig. 4b). The broad emission band observed in the blue-green region is due to surface states and trapping centers for electron hole pairs which originated from O-, N-, and S- containing groups of CQDs. The cluster luminescence responsible for the blue green emission bands of CNP is formed by the aggregation of heteroatoms containing functional groups attached to the surface states via weak forces [47,48]. While carbon core with cluster of surface states acts as the center of blue green luminescence, the strong red luminescence observed can be ascribed to the molecular state transitions associated with chlorophyll and pheophytin [45,49]. Addition of PVP enhanced the red emission intensity by about 8 times in carbon nanoparticles due to molecular state transitions. Increase in red emission is accompanied by decrease in blue emission which indicates energy transfer from carbon core to porphyrin rings. Due to the presence of intense red emission, the blue-green emitting CN could turn into a good white light emitter as shown in the inset of Fig. 4b.

From Fig. 5, it can be observed that excitation spectrum of CN and CNP overlaps with blue-green emission and a donor-acceptor pair is established between carbon nuclei and porphyrin. Additionally, it can be inferred that characteristic excitation peaks of pheophytin are enhanced in CNP which suggests the interaction between PVP and pheophytin. Moreover, in presence of PVP, the average exciton life time of blue green emission peaked at 480 nm is decreased while average decay time of red emission peaked at 665 nm is increased (Table. 1). This confirms the

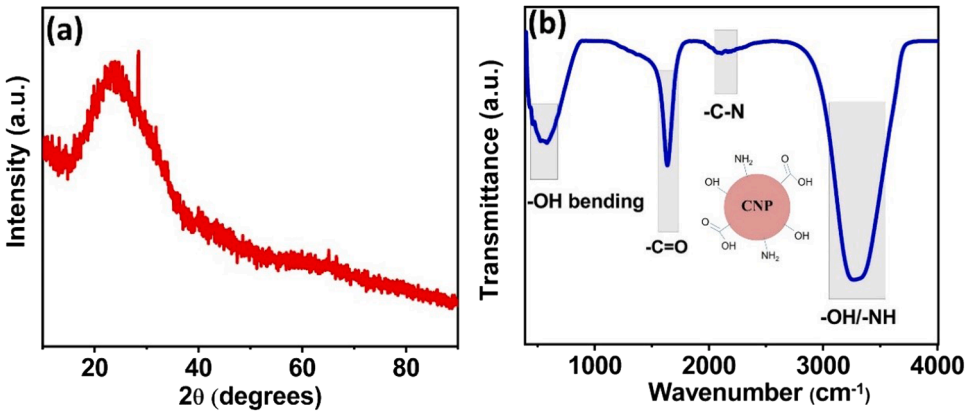

Fig. 1. (a) XRD pattern and (b) FTIR spectrum of CNP; the inset of the figure (b) shows the structure of surface functionalized carbon nanoparticles.

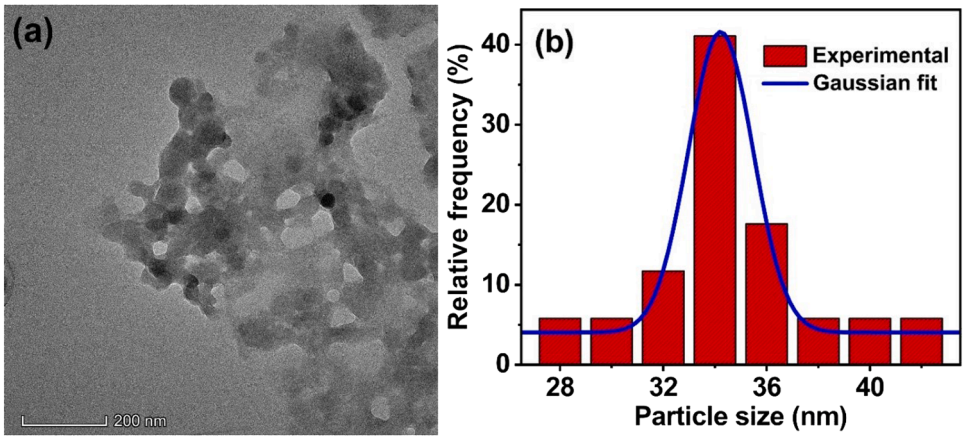

Fig. 2. (a) TEM image of CNP and (b) corresponding particle size distribution.

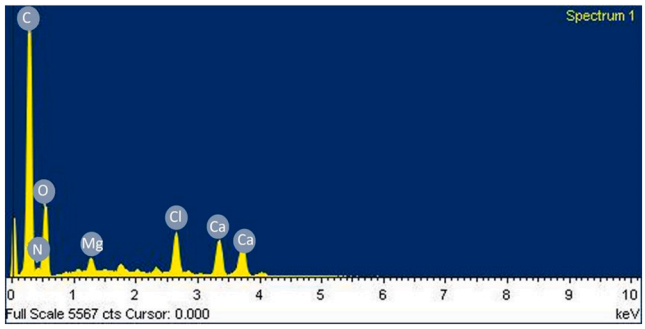

Fig. 3. EDS spectrum of CNP.

energy transfer between carbon nuclei and porphyrin from chlorophyll/pheophytin to obtain enhanced red emission.

It was reported that carbon quantum dots synthesized from withered leaves emit blue color while those prepared from green leaves exhibit dual blue-red emission [50]. Here, the leaves are air dried at room temperature using a hairdryer, which causes degradation of chlorophyll compared to fresh leaves. This results in less surface modification of CN by chlorophyll derived porphyrin groups. Additionally, when the leaves are dried at 90 °C and crushed for synthesis, the red emission is almost quenched (Fig. S1). This reduction in red emission is due to decrease in the amount of chlorophyll and pheophytin. To investigate dependence of leaf drying temperature, PL spectra of carbon nanoparticles (Fig. S2) prepared by air dried leaves (~40 °C) (CN), with leaves dried at oven at 60 °C (CN-60) and at 90 °C (CN-90), respectively are studied. As the leaf drying temperature increases, chlorophyll/pheophytin content in the leaves decreases remarkably which is accompanied with the reduction in red luminescence. Additionally, as drying temperature increases, high degree of carbonization occurs which helps CN-90 to exhibit greater blue green emission intensity. However, PVP could form complexes with porphyrin compounds through hydrogen bonds or coordination bonds which are capable of photoinduced electron transfer [51]. From the excitation spectrum (Fig. S3) it is clear that addition of PVP causes partial conversion of chlorophyll to pheophytin. Moreover, the presence of characteristic peaks at 505 and 535 nm suggests the absence of any other metal substituted derivatives of chlorophyll. Even though chlorophyll and pheophytin has characteristic red emission peaked at 665 nm wavelength [49] excitation spectra for chlorophyll and pheophytin for 665 nm has different characteristic absorption peaks. While absorption band peaked at 405, 435 and 604 nm is characteristic excitations of chlorophyll, the peaks at 405, 505 and 534 nm can be attributed to prominent excitation peaks pheophytin emission. This confirms the existence of porphyrin containing chlorophyll and pheophytin on CNP. Thus, direct thermal decomposition of organics from dried leaves in the presence of PVP gives carbon nanoparticles with surface functionalized with porphyrins from chlorophyll and pheophytin. The schematic representation depicting the synthesis of such dual emissive carbogenic nanoparticles has been shown in Fig. 6. The presence of PVP effectively functionalizes the CNP surface with more porphyrin groups to absorb more in the visible region (400–700 nm). Moreover, these molecular states are predominantly responsible for the enhanced bright red emission in CNPs under UV excitation [50,52].

The room-temperature photoluminescence quantum yield (QY) is obtained as 0.81 which can be attributed occurrence of less passivated

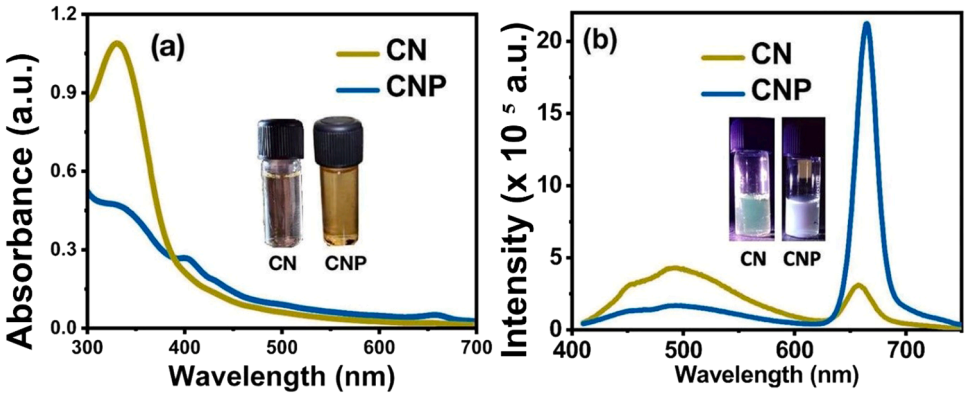

Fig. 4. (a) UV-visible absorption spectra of CN and CNP (b) fluorescence spectra of CN and CNP at 390 nm excitation wavelength (inset of Fig. 4a and b shows the photographs of CN and CNP solution in daylight and under UV excitation, respectively).

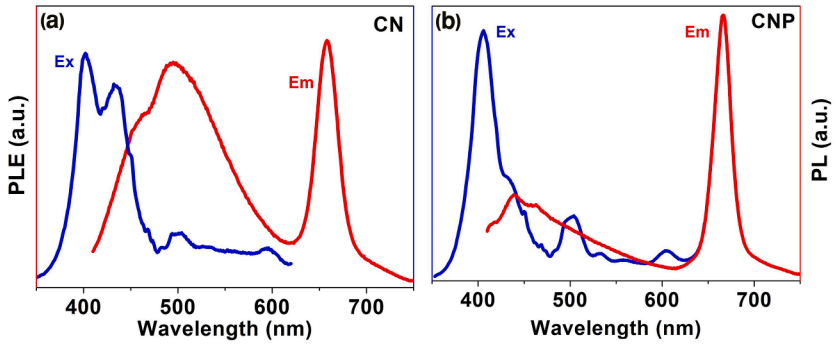

Fig. 5. Photoluminescence excitation spectra (Blue line) and Photoluminescence emission spectra (red line) of (a) CN and (b) CNP, respectively.

Table. 1
The fluorescence life time parameters of CNP monitored for blue green (B-G) and red (R) peak.

Sample code	α_1	τ_1 (ns)	α_2	τ_2 (ns)	α_3	τ_3 (ns)	T_{avg} (ns)
CN - (B-G peak)	1.237	0.678	0.241	2.587	0.035	0.581	0.979
CN - (R peak)	0.429	3.971	0.377	4.085	0.365	0.834	3.029
CNP- (B-G peak)	0.713	0.733	0.682	0.361	0.325	1.624	0.753
CNP – (R peak)	0.300	3.072	0.266	4.712	0.235	5.743	4.400

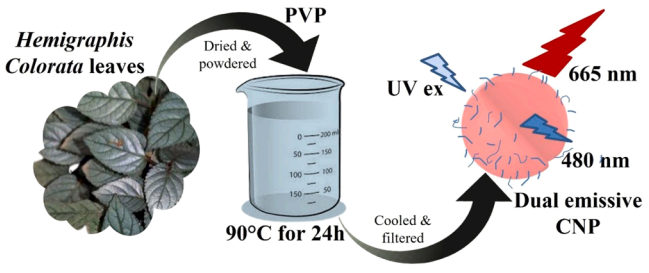

Fig. 6. Synthesis of dual emissive CNP from *Hemigraphis colorata* leaves.

surface states and defects in prepared CNP at low pyrolysis temperature. This results in defect-mediated nonradiative recombination from surface states and trap sites [53]. Increase in the pyrolysis temperature can increase the QY of nanoparticles, but temperature beyond 100 °C cause degradation of chlorophyll and pheophytin. Similar QY values have been reported for certain carbon nanoparticles [54] due to the presence of surface states and defects.

The Fig. 7a shows the fluorescence of the CN upon varying excitation wavelength. Interestingly, the blue peak has an apparent excitation dependent emission with peak center varying from 475 to 510 nm while the red peak shows an excitation independent emission peak centered at 665 nm. Also, the intensity of the peak centered at 480 nm is almost the same with the peak centered at 665 nm wavelength. Upon different excitation wavelengths, blue-green emission together with the narrow red emission band could exhibit color varying from light blue to greenish yellow as obtained from CIE 1931 chromaticity chart of CN.

Subsequently, as observed for CN, the low energy emission peak at 655 nm wavelength is narrow and excitation independent (Fig. 8) for PVP capped carbon nanoparticles. As seen from the inset of Fig. 8a, the blue- green emission is broad and excitation dependent like exhibited by CN. Upon different excitation wavelengths from 370 to 420 nm, tunable dual-band emission gives white to yellow color as obtained from the CIE 1931 chromaticity chart of CNP. The CIE chromaticity coordinates obtained for all excitations from 370 to 420 nm confirms that the fluorescence obtained from CNP under broad excitation wavelengths lies in white light trajectory (Table S1). As nanoparticles suffer aggregation induced quenching, the concentration effect of the nanoparticles is studied by analyzing the fluorescence spectra of CNP at varying volume % (1–4) of carbon nanoparticles (Fig. 8c). According to Chen, the fluorescence band is red shifted at higher concentrations of nanoparticles [55]. It is evident that there is no discernible shift in major peak position of both fluorescence bands, upon varying concentration of the nanoparticles. This is due to the effective wrapping of nanoparticles with PVP. The intensity of the PL spectral peak is maximum for an intermediate concentration (3 vol% carbon nanoparticles) and decreases slightly with increase of concentration. As concentration is increased there will be higher number of particles and spacing between the particles will be less than the Förster distance (R_0). This might cause

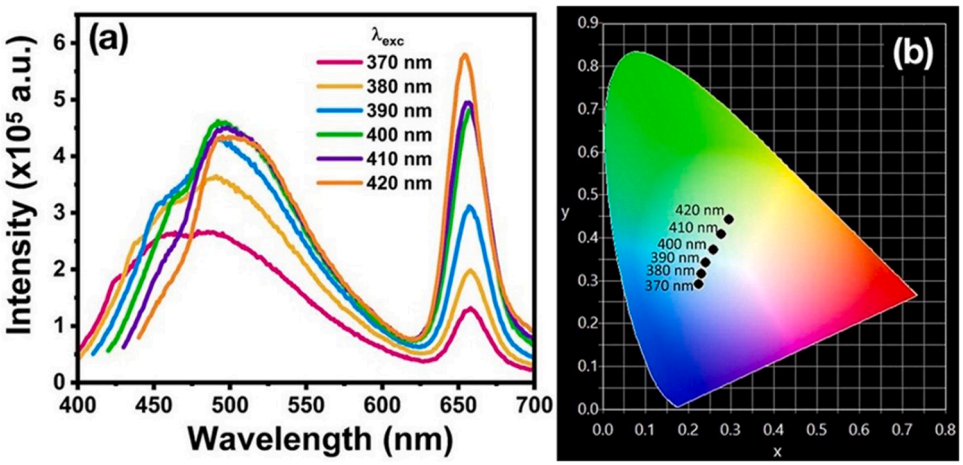

Fig. 7. (a) Excitation wavelength dependent emission spectra and (b) CIE 1931 chromaticity chart of CN.

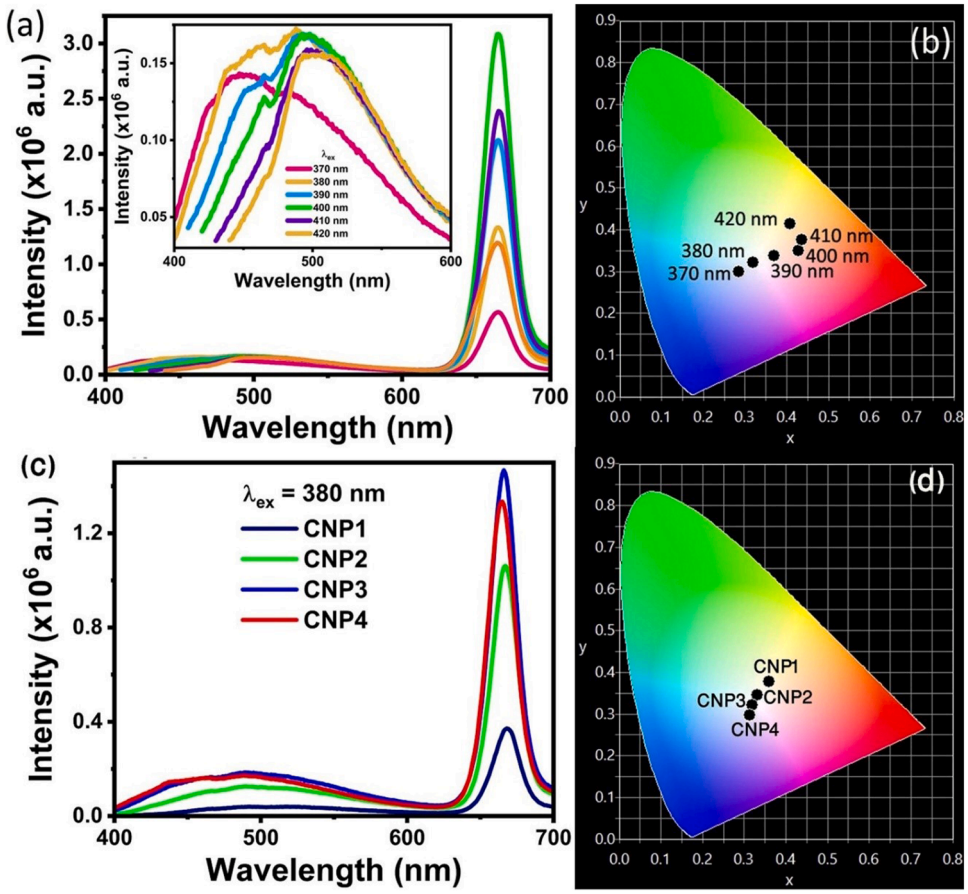

Fig. 8. (a) Excitation wavelength dependent emission spectra of CNP (b) CIE 1931 chromaticity chart of CNP, (c) Emission spectra of CNP at varying volume% (1–4) of carbon nanoparticles (CNP1 to CNP4) at 380 nm excitation and (d) corresponding CIE 1931 chromaticity chart.

reabsorption of emission which results in self-quenching of the fluorescence. Moreover, an increase in the number of particles results in aggregation induced quenching which can also affect the fluorescence efficiency.

Tunable correlated color temperature (CCT) values from warm to cool emission are obtained upon different excitation wavelengths (Fig. S4). At 400 nm excitation wavelength, all concentrations give warm white color emission (2500 K) which changes to cool white color emission at UV excitations (4623–8117 K). Inspired by the excellent tunability for CCT and CIE color coordinates, cool white emissions are obtained for CNP (Fig. 9a) at 370 nm excitation wavelength. White emissions having CIE color coordinates (0.2860, 0.2983) with CCT of 8980 K and CRI value of 68 are achieved for CNP (3 vol% carbon nanoparticles) and is marked in CIE 1931 color space (Fig. 9b). The color point lies on the black body Planckian locus. For the sake of overcoming the agglomeration of nanoparticles, solid matrix of CNP - silica xerogels were fabricated and white emissions are observed (inset of Fig. 9a).

To check the stability of CNP solutions in normal room temperature, the temporal stability of the PL intensity of CNP was evaluated for an interval of one week (Fig. 10a). It can be identified that the intensity of

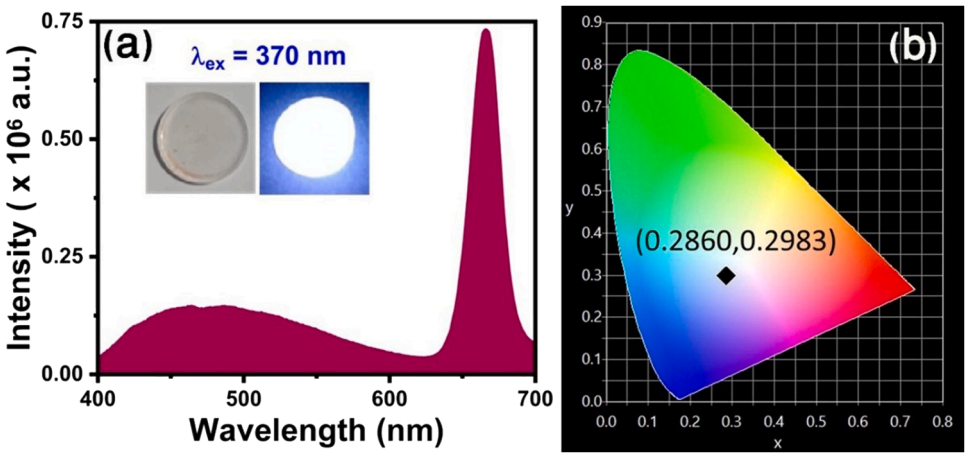

Fig. 9. (a) PL spectra of CNP at excitation wavelength of 370 nm showing dual emission at 480 nm and 665 nm; the inset shows the photograph of silica glass dipped in CNP under daylight and UV illumination (b) CIE plot of PL emission from CNP exhibiting indices values (0.2860, 0.2983).

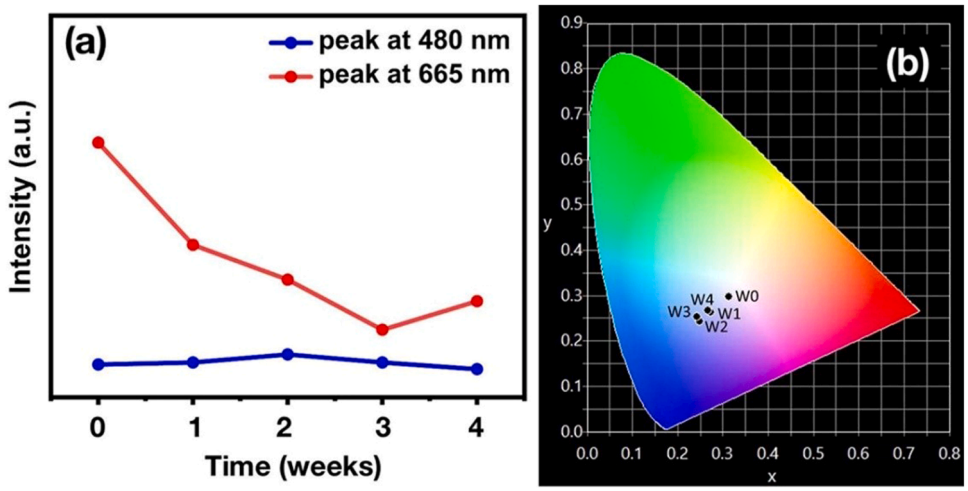

Fig. 10. (a) Plot of PL intensity maximum of CNP solution and storage time. (B) corresponding CIE plot.

the blue peak at 480 nm stays relatively constant. Even though the peak at 665 nm shows a slight decrease in PL intensity, it remains almost the same after the second week of storage. From the CIE 1931 color space, it is evident that the white emission remains unchanged for a period of 4 weeks. All the results demonstrate the enormous potential applications of the biomass derived CQD-based phosphors in high-performance WLEDs.

4. Conclusion

Dual emitting carbon nanoparticles were prepared through one step, facile, low temperature thermal degradation of *Hemigraphis colorata* leaves. Detailed characterizations proved that nanoparticles have an average size range of 28–42 nm. The surface states of nanoparticles are rich in electron donating groups and porphyrin groups, ultimately determining the dual color of their PL, which peaked at 480 and 665 nm wavelengths. With the addition of PVP, the intensity of red emission enhances sharply. While the blue emission band was excitation dependent, the red emission band was excitation independent. This strategy elucidates the design of efficient white light emitting devices with broad band excitation. Upon different excitation wavelengths, dual emissive carbon nanoparticles could show tunable correlated color temperature (CCT) values from warm to cool emission which promises for environment-friendly, indoor, and outdoor lighting applications.

Declaration of Competing Interest

The authors declare that they have no known competing financial interests or personal relationships that could have appeared to influence the work reported in this paper.

Data availability

Data will be made available on request.

Acknowledgments

The authors are extremely grateful to the TEM facility at center for Nano and Soft Matter Sciences, Bengaluru. We also thank DST-FIST supported Central Instrumentation Facilities, St. Thomas College, Thrissur, India for the services and characterization facilities provided.

Supplementary materials

Supplementary material associated with this article can be found, in the online version, at doi:10.1016/j.cartre.2023.100296.

References

[1] E.F. Schubert, J.K. Kim, Solid-state light sources getting smart, Science 308 (5726) (2005) 1274–1278, https://doi.org/10.1126/science.1108712. May.

[2] B.W. D'Andrade, S.R. Forrest, White organic light-emitting devices for solid-state lighting, Adv. Mater. 16 (18) (2004) 1585–1595, https://doi.org/10.1002/adma.200400684.

[3] A.K. Bedyal, V. Kumar, H.C. Swart, Charge compensated derived enhanced red emission from $Sr_3(VO_4)2:Eu_{3+}$ nanophosphors for white light emitting diodes and flat panel displays, J. Alloy. Compd. 709 (2017) 362–372, https://doi.org/10.1016/j.jallcom.2017.03.139. Jun.

[4] J. Wang, W. Lin, W. Li, Three-channel fluorescent sensing via organic white light-emitting dyes for detection of hydrogen sulfide in living cells, Biomaterials 34 (30) (2013) 7429–7436, https://doi.org/10.1016/j.biomaterials.2013.06.013. Oct.

[5] Y.P. Xia, et al., Utilizing an effective framework to dye energy transfer in a carbazole-based metal–organic framework for high performance white light emission tuning, Inorg. Chem. Front. 5 (11) (2018) 2868–2874, https://doi.org/10.1039/C8QI00747K. Nov.

[6] H. Chen, et al., Chromaticity-tunable phosphor-in-glass for long-lifetime high-power warm w-LEDs, J. Mater. Chem. C 3 (31) (2015) 8080–8089, https://doi.org/10.1039/C5TC01057H. Jul.

[7] T. Wang, V. Chirmanov, W.H.M. Chiu, P.V. Radovanovic, Generating tunable white light by resonance energy transfer in transparent dye-conjugated metal oxide nanocrystals, J. Am. Chem. Soc. 135 (39) (2013) 14520–14523, https://doi.org/10.1021/ja407013z. Oct.

[8] Q.L. Chen, C.F. Wang, S. Chen, One-step synthesis of yellow-emitting carbogenic dots toward white light-emitting diodes, J. Mater. Sci. 48 (6) (2013) 2352–2357, https://doi.org/10.1007/s10853-012-7016-8. Mar.

[9] Y. Zhang, et al., Employing heavy metal-free colloidal quantum dots in solution-processed white light-emitting diodes, Nano Lett. 11 (2) (2011) 329–332, https://doi.org/10.1021/nl1021442. Feb.

[10] X. Feng, Y. Zhang, A simple and green synthesis of carbon quantum dots from coke for white light-emitting devices, RSC Adv. 9 (58) (2019) 33789–33793, https://doi.org/10.1039/C9RA06946A.

[11] V. Revuri, K. Cherukula, M. Nafiujjaman, K. Jae cho, I.K. Park, Y.K. Lee, White-light-emitting carbon nano-onions: a tunable multichannel fluorescent nanoprobe for glutathione-responsive bioimaging, ACS Appl. Nano Mater. 1 (2) (2018) 662–674, https://doi.org/10.1021/acsanm.7b00143. Feb.

[12] K.J. Chen, et al., White light emitting diodes with enhanced CCT uniformity and luminous flux using ZrO_2 nanoparticles, Nanoscale 6 (10) (2014) 5378–5383, https://doi.org/10.1039/C3NR06894C. Apr.

[13] S. Bose, et al., Synthesis of silicon nanoparticles from rice husk and their use as sustainable fluorophores for white light emission, ACS Sustain. Chem. Eng. 6 (5) (2018) 6203–6210, https://doi.org/10.1021/acssuschemeng.7b04911. May.

[14] H.T. Nicolai, A. Hof, P.W.M. Blom, Device physics of white polymer light-emitting diodes, Adv. Funct. Mater. 22 (10) (2012) 2040–2047, https://doi.org/10.1002/adfm.201102699.

[15] Y. Tang, W. Cao, L. Yao, Y. Cui, Y. Yu, G. Qian, Polyurethane-coated luminescent dye@MOF composites for highly-stable white LEDs, J. Mater. Chem. C 8 (35) (2020) 12308–12313, https://doi.org/10.1039/D0TC02887H. Sep.

[16] C.Y. Sun, et al., Efficient and tunable white-light emission of metal–organic frameworks by iridium-complex encapsulation, Nat. Commun. 4 (1) (2013), https://doi.org/10.1038/ncomms3717. Art. no. 1Nov.

[17] Y. Ledemi, et al., White light and multicolor emission tuning in triply doped Yb3+/Tm3+/Er3+ novel fluoro-phosphate transparent glass-ceramics, J. Mater. Chem. C 2 (25) (2014) 5046–5056, https://doi.org/10.1039/C4TC00455H. Jun.

[18] W. Ki, J. Li, G. Eda, M. Chhowalla, Direct white light emission from inorganic–organic hybrid semiconductor bulk materials, J. Mater. Chem. 20 (47) (2010) 10676–10679, https://doi.org/10.1039/C0JM02213F. Nov.

[19] S. Wang, et al., A semi-conductive organic–inorganic hybrid emits pure white light with an ultrahigh color rendering index, J. Mater. Chem. C 5 (19) (2017) 4731–4735, https://doi.org/10.1039/C7TC00279C. May.

[20] H. Li, Z. Kang, Y. Liu, S.T. Lee, Carbon nanodots: synthesis, properties and applications, J. Mater. Chem. 22 (46) (2012) 24230–24253, https://doi.org/10.1039/C2JM34690G. Nov.

[21] J. Liu, R. Li, B. Yang, Carbon dots: a new type of carbon-based nanomaterial with wide applications, ACS Cent. Sci. 6 (12) (2020) 2179–2195, https://doi.org/10.1021/acscentsci.0c01306. Dec.

[22] M. Semeniuk, et al., Future perspectives and review on organic carbon dots in electronic applications, ACS Nano 13 (6) (2019) 6224–6255, https://doi.org/10.1021/acsnano.9b00688. Jun.

[23] M.J. Krysmann, A. Kelarakis, P. Dallas, E.P. Giannelis, Formation mechanism of carbogenic nanoparticles with dual photoluminescence emission, J. Am. Chem. Soc. 134 (2) (2012) 747–750, https://doi.org/10.1021/ja204661r. Jan.

[24] A. Nandy, A. Kumar, S. Dwivedi, S.K. Pal, D. Panda, Connecting the dots of carbon nanodots: excitation (in)dependency and white-light emission in one-step, J. Phys. Chem. C 123 (33) (2019) 20502–20511, https://doi.org/10.1021/acs.jpcc.9b02428. Aug.

[25] C. Testa, A. Zammataro, A. Pappalardo, G.T. Sfrazzetto, Catalysis with carbon nanoparticles, RSC Adv. 9 (47) (2019) 27659–27664, https://doi.org/10.1039/C9RA05689K.

[26] R. Santonocito, M. Intravaia, I.M. Caruso, A. Pappalardo, G.T. Sfrazzetto, N. Tuccitto, Fluorescence sensing by carbon nanoparticles, Nanoscale Adv. 4 (8) (2022) 1926–1948, https://doi.org/10.1039/D2NA00080F.

[27] E. Asadian, M. Ghalkhani, S. Shahrokhian, Electrochemical sensing based on carbon nanoparticles: a review, Sens. Actuators B Chem. 293 (2019) 183–209, https://doi.org/10.1016/j.snb.2019.04.075. Aug.

[28] H. Li, et al., Recent advances in carbon dots for bioimaging applications, Nanoscale Horiz. 5 (2) (2020) 218–234, https://doi.org/10.1039/C9NH00476A.

[29] R. Kumari, K. Pal, P. Karmakar, S.K. Sahu, pH-responsive Mn-doped carbon dots for white-light-emitting diodes, fingerprinting, and bioimaging, ACS Appl. Nano Mater. 2 (9) (2019) 5900–5909, https://doi.org/10.1021/acsanm.9b01335. Sep.

[30] K. Ahmad, A. Pal, U.N. Pan, A. Chattopadhyay, A. Paul, Synthesis of single-particle level white-light-emitting carbon dots via a one-step microwave method, J. Mater. Chem. C 6 (25) (2018) 6691–6697, https://doi.org/10.1039/C8TC01276H. Jun.

[31] X. Chen, et al., Blue and green double band luminescent carbon quantum dots: synthesis, origin of photoluminescence, and application in white light-emitting devices, Appl. Phys. Lett. 118 (15) (2021), 153102, https://doi.org/10.1063/5.0046495. Apr.

[32] H. Qi, et al., Synthesis of multiple-color emissive carbon dots towards white-light emission, Nanotechnology 31 (24) (2020), 245001, https://doi.org/10.1088/1361-6528/ab7b08. Mar.

[33] T.C. Wareing, P. Gentile, A.N. Phan, Biomass-based carbon dots: current development and future perspectives, ACS Nano 15 (10) (2021) 15471–15501, https://doi.org/10.1021/acsnano.1c03886. Oct.

[34] X. Zhang, et al., Natural-product-derived carbon dots: from natural products to functional materials, ChemSusChem 11 (1) (2018) 11–24, https://doi.org/10.1002/cssc.201701847.

[35] V. Singh, A.K. Mishra, White light emission from vegetable extracts, Sci. Rep. 5 (1) (2015). Accessed: Apr. 15, 2023. [Online]. Available, https://www.cabdirect.org/cabdirect/abstract/20163161902.

[36] J. Mathew, J. Joy, A.S. Kumar, J. Philip, White light emission by energy transfer from areca nut husk extract loaded with carbon dots synthesized from the same extract, J. Lumin. 208 (2019) 356–362, https://doi.org/10.1016/j.jlumin.2018.10.110. Apr.

[37] V. Singh, A.K. Mishra, White light emission from a mixture of pomegranate extract and carbon nanoparticles obtained from the extract, J. Mater. Chem. C 4 (15) (2016) 3131–3137, https://doi.org/10.1039/C6TC00480F. Apr.

[38] B. Kumar, M. Vijayakumar, R. Govindarajan, P. Pushpangadan, Ethnopharmacological approaches to wound healing—exploring medicinal plants of India, J. Ethnopharmacol. 114 (2) (2007) 103–113, https://doi.org/10.1016/j.jep.2007.08.010. Nov.

[39] M.I. Safna, U.V. Visakh, A. Gangadharan, Biological activity of hexane extract of Hemigraphis colorata, an indigenous wound healing plant, Mater. Today Proc. 25 (2020) 294–297, https://doi.org/10.1016/j.matpr.2020.01.461. Jan.

[40] V.G. Nandakumar, S. Suresh, C.O. Sreekala, S.K. Sudheer, V.P. Mahadevan Pillai, Hemigraphis colorata as a natural dye for solar energy conversion, Mater. Today Proc. 4 (2) (2017) 4358–4365, https://doi.org/10.1016/j.matpr.2017.04.006. Part CJan.

[41] T.N.J.I. Edison, R. Atchudan, M.G. Sethuraman, J.J. Shim, Y.R. Lee, Microwave assisted green synthesis of fluorescent N-doped carbon dots: cytotoxicity and bio-imaging applications, J. Photochem. Photobiol. B 161 (2016) 154–161, https://doi.org/10.1016/j.jphotobiol.2016.05.017. Aug.

[42] A. Dager, A. Baliyan, S. Kurosu, T. Maekawa, M. Tachibana, Ultrafast synthesis of carbon quantum dots from fenugreek seeds using microwave plasma enhanced decomposition: application of C-QDs to grow fluorescent protein crystals, Sci. Rep. 10 (1) (2020), https://doi.org/10.1038/s41598-020-69264-9. Art. no. 1, Jul.

[43] J. Song, Q. Ma, Y. Liu, Y. Guo, F. Feng, S. Shuang, Novel single excitation dual-emission carbon dots for colorimetric and ratiometric fluorescent dual mode detection of Cu^{2+} and Al^{3+} ions, RSC Adv. 9 (66) (2019) 38568–38575, https://doi.org/10.1039/C9RA07030C.

[44] K.J. Mintz, Y. Zhou, R.M. Leblanc, Recent development of carbon quantum dots regarding their optical properties, photoluminescence mechanism, and core structure, Nanoscale 11 (11) (2019) 4634–4652, https://doi.org/10.1039/C8NR10059D.

[45] X. Xu, et al., Red-emissive carbon dots from spinach: characterization and application in visual detection of time, J. Lumin. 227 (2020), 117534, https://doi.org/10.1016/j.jlumin.2020.117534. Nov.

[46] L. Tang, et al., Deep ultraviolet photoluminescence of water-soluble self-passivated graphene quantum dots, ACS Nano 6 (6) (2012) 5102–5110, https://doi.org/10.1021/nn300760g. Jun.

[47] S. Wang, et al., Cluster-luminescent polysiloxane nanomaterials: adjustable full-color ultralong room temperature phosphorescence and a highly sensitive response to silver ions, Inorg. Chem. Front. 9 (14) (2022) 3619–3626, https://doi.org/10.1039/D2QI00914E. Jul.

[48] H. Qi, et al., Rationally designed matrix-free carbon dots with wavelength-tunable room-temperature phosphorescence, Chem. Asian J. 18 (6) (2023), e202201284, https://doi.org/10.1002/asia.202201284.

[49] T. Galeano Díaz, I. Durán Merás, C.A. Correa, B. Roldán, M.I. Rodríguez Cáceres, Simultaneous fluorometric determination of chlorophylls a and b and pheophytins a and b in olive oil by partial least-squares calibration, J. Agric. Food Chem. 51 (24) (2003) 6934–6940, https://doi.org/10.1021/jf034456m. Nov.

[50] H. Rao, et al., Smartphone-based fluorescence detection of Al^{3+} and H_2O based on the use of dual-emission biomass carbon dots, ACS Sustain. Chem. Eng. 8 (23) (2020) 8857–8867, https://doi.org/10.1021/acssuschemeng.0c03354. Jun.

[51] Y. Cao, T. Takasaki, S. Yamashita, Y. Mizutani, A. Harada, H. Yamaguchi, Control of photoinduced electron transfer using complex formation of water-soluble porphyrin and polyvinylpyrrolidone, Polymers 14 (6) (2022), https://doi.org/10.3390/polym14061191 (Basel)Art. no. 6, Jan.

[52] W. Li, et al., Enhanced biological photosynthetic efficiency using light-harvesting engineering with dual-emissive carbon dots, Adv. Funct. Mater. 28 (44) (2018), 1804004, https://doi.org/10.1002/adfm.201804004.
[53] S. Wang, et al., A 200-fold quantum yield boost in the photoluminescence of silver-doped AgxAu25−x nanoclusters: the 13th silver atom matters, Angew. Chem. 126 (9) (2014) 2408–2412, https://doi.org/10.1002/ange.201307480.
[54] H. Kim, D.H. Lien, M. Amani, J.W. Ager, A. Javey, Highly stable near-unity photoluminescence yield in monolayer MoS_2 by fluoropolymer encapsulation and superacid treatment, ACS Nano 11 (5) (2017) 5179–5185, https://doi.org/10.1021/acsnano.7b02521. May.
[55] J. Zhu, et al., Carbon dots with efficient solid-state red-light emission through the step-by-step surface modification towards light-emitting diodes, Dalton Trans. 47 (11) (2018) 3811–3818, https://doi.org/10.1039/C7DT04579D. Mar.